Chapter 5
Mesoscopic Studies of Nanofluid Dynamic Wetting: From Nanoscale to Macroscale

Abstract In this chapter, a lattice Boltzmann method with some simple but effective treatments with consideration of nanofluid surface tension and rheology modification, as well as the nanoparticle sedimentations, is conducted to investigate the effects of nanoparticle kinetics at the nanoscale (10^{-9} m) on the dynamic wetting behaviors occurring at the macroscopic scale (10^{-3} m). The study provides multi-scale understanding and guidelines to tune the nanofluid dynamic wetting behaviors.

5.1 Introduction

The mechanism of dynamic wetting by nanofluids is still unclear due to the complicated dynamic wetting behaviors, as well as the limitations of nanoscale experimental techniques and fundamental theories. In one aspect, the contact line motion is driven by the viscous force and surface tension force, which relate to the viscosity and surface tension of the spreading fluid. The nanoparticle motion in nanofluids significantly changes the surface tension, viscosity, and rheology of the base fluids [1, 2]. Therefore, the modification of the surface tension and the rheology by adding nanoparticles strongly affects the nanofluid dynamic wetting, which has been discussed as the bulk dissipation in Chap. 4. In other aspect, the suspensions of millions of nanoparticle induce a large amount of solid–liquid surface energy in nanofluids. To make the system steady, it is natural for nanoparticles to aggregate or self-assemble in the nanofluids to reach the lowest free energy state. The nanoparticle self-assembly near the contact line region strongly affects the contact line motion, leading to the nanofluid "super-spreading" behaviors [3], which has been discussed as the local dissipation in Chap. 3. The self-assembly of nanoparticles in the vicinity of the contact line region induces an additional disjoining pressure, braking the force balance at the contact line, and hence facilitating the motion of contact line [3–6]. The nanofluid "super-spreading" was widely used to explain the extraordinary nanofluid evaporation [7, 8] and boiling

G. Lu, *Dynamic Wetting by Nanofluids*,
Springer Theses, DOI 10.1007/978-3-662-48765-5_5

[9–11]. Do these three effects, surface tension modification, rheology modification, and self-assembly, affect the dynamic wetting behavior individually or jointly? The answers to this question will reveal the mechanism of nanofluid dynamic wetting or provide the guideline to tune the nanofluid wetting kinetics. However, the study of the dynamic wetting by nanofluids is of great challenge since the wetting behavior crosses several length and timescales. Both the bulk and the local dissipation due to nanoparticle motions and self-assembly occur in the nanoscale. However, the spreading droplets usually have several millimeters in diameters. The difference between these two length scales is as large as several million times, from 10^{-9} to 10^{-3} m. Multiscale experimental techniques and fundamental theories are still insufficient to provide good understanding for these multiscale problems. The Lattice Boltzmann method (LBM) has been regarded as a very promising method to simulate the multiscale problems. The LBM is based on mesoscopic kinetic equations (the Boltzmann equation). The Navier–Stokes equations that describe the macroscopic flow problems can be derived from the Boltzmann equation using the Chapman–Enskog multiscale expansion. Due to the intrinsic microscopic kinetics, the LBM was widely used to investigate the flow and heat transfer of nanofluids [12–24] or pure fluid dynamic wetting [25–29]. However, there are few studies on the nanofluid dynamic wetting, especially the multiscale mechanisms from nanoparticle motions to macroscopic dynamic wetting.

In this chapter, the effects of nanoscale dissipations due to nanoparticle kinetics on the macroscopic dynamic wetting were studied from the viewpoint of mesoscopic simulations. The nanoscale dissipations contain the bulk dissipation, due to the nanoparticle motion in the bulk liquid, and the local dissipation due to the self-assembly of nanoparticles in the vicinity of the contact line regions. The roles of nanoparticle bulk and local dissipations on the macroscopic dynamic wetting were investigated by examining the individual or coupled effects of nanofluid surface tension, rheological properties, and nanoparticle self-assembly modes. The study provides multiscale understanding and tunable methods of the nanofluid dynamic wetting.

5.2 Simulation Models

5.2.1 Geometry Model

The simulated schematic is shown in Fig. 5.1. A 2D lattice grid was used to simulate a droplet spreading on an ideal and smooth solid surface. Three grid sizes, (I) 500×100 lu^2 (lattice unit, lu), (II) 1000×200 lu^2, and (III) 2000×400 lu^2 were used to test the grid independence, as shown in Fig. 5.1b. The moderate grid of 1000×200 lu^2 was used by considering both accuracy and efficiency. The droplet initial radius is $R_0 = 50$ lu. The left side and the right side are the period boundary conditions. The bounce-back condition is applied at the top side.

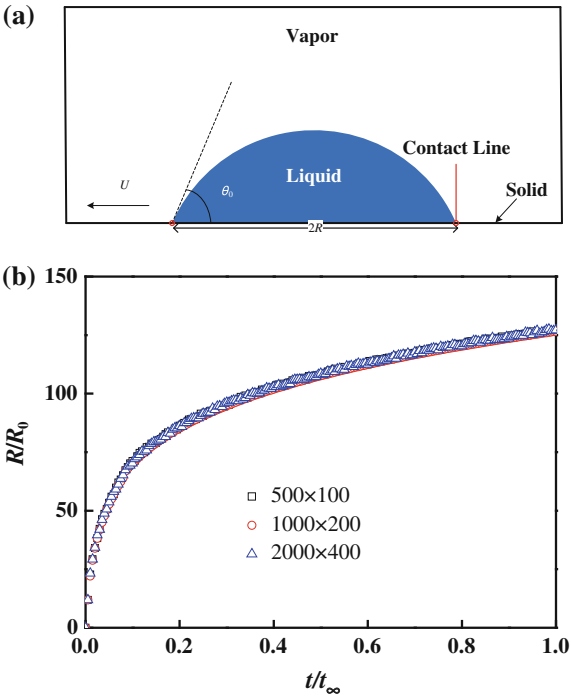

Fig. 5.1 Simulation geometry and lattice grid test. **a** Simulation geometry. **b** Lattice grid test

5.2.2 *Dynamic Wetting with Triple-Phase Contact Line Motions*

The droplet dynamic wetting is a replacement process of the liquid over the vapor on the solid surface, including interactions between the solid, the liquid, and the vapor surfaces. The multiphase LBM was used to simulate the replacement processes between the liquid and the vapor, including all the interactions between the solid–vapor, solid–liquid, vapor–vapor, liquid–liquid, and liquid–vapor.

A D2Q9 LBM model with Bhatnagar–Gross–Krook (BGK) collision operator was used to simulate the fluid flow [30]. To simulate multiphase fluids (liquid and vapor), the long-range interactions for liquid–liquid, vapor–vapor, and liquid–vapor are described using the Shan-Chen model [31–33]:

$$F(\mathbf{x},t) = -G\psi(\mathbf{x},t)\sum_{\alpha=1}^{8} w_\alpha \psi(\mathbf{x}+\mathbf{e}_\alpha \Delta t, t)\mathbf{e}_\alpha, \tag{5.1}$$

where G is the interaction strength and ψ is the interaction potential expressed as [34]:

$$\psi(\rho) = \psi_0 \exp\left(\frac{-\rho_0}{\rho}\right), \tag{5.2}$$

where ψ_0 and ρ_0 are constants, usually with the values of 4 and 200 [35].

The dynamic wetting of fluids on the solid surfaces is governed by an adhesive interaction force between the fluid (liquid or vapor) and the solid surface [36]:

$$F_{\text{ads}}(\mathbf{x}, t) = -G_{\text{ads}}\psi(\mathbf{x}, t)\sum_{\alpha=1}^{8} w_\alpha s(\mathbf{x} + \mathbf{e}_\alpha \Delta t, t)\mathbf{e}_\alpha, \tag{5.3}$$

where G_{ads} is the adsorption coefficient, which is 327 in this study. s is a switch parameter with the value of 1, if the neighbor lattice of the fluid lattice is a solid boundary and 0 for a neighbor fluid lattice.

5.2.3 *Nanofluid Modeling*

Figure 5.2 shows the two nanoparticle dissipation mechanisms due to the nanoparticle motion and the self-assembly: bulk dissipation and local dissipation. In the bulk dissipation, nanoparticles distribute homogeneously in the bulk liquids. Therefore, it is reasonable to assume that the nanofluids are homogeneous single-phase. The nanoparticles were treated as "fluid" lattices. The particle–particle and particle–fluid interactions are still cohesive forces, which can be calculated with Eq. (5.1) with different G. In the simulations, G switches to the particle–fluid/particle–particle value if the lattice or the neighbor lattice is occupied by a nanoparticle lattice. The nanoparticles only modify the surface tension and rheology of the base fluids if the bulk dissipation occurs only. For the local dissipation, the nanoparticle lattices deposit at a given deposition rate to the bottom or to the vicinity of the contact line region during the droplet spreading, changing the thickness of liquid film and then resulting the additional disjoining pressures, which brake the resultant forces and then facilitate the motion of contact line.

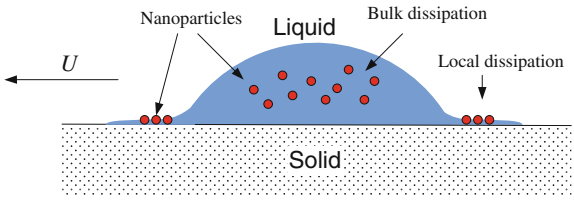

Fig. 5.2 Schematic of the two nanoparticle dissipations of nanofluid dynamic wetting

5.2.3.1 Bulk Dissipation Due to the Surface Tension and Rheology Modification

The nanoparticles significantly modify the surface tension of nanofluids, which strongly affects the dynamic wetting process [37]. The nanoparticles can increase or reduce the surface tension of base fluids, which depends on the interactions between nanoparticles and solvent molecules. The molecular dynamic simulations show that the nanoparticle wettability is responsible for the surface tension modifications [38]. Hydrophobic nanoparticles always tend to stay on the free surface so they behave like a surfactant to reduce the surface tension. Hydrophilic nanoparticles immerge into the bulk fluid which increases the surface tension of the nanofluids. Thus, at mesoscopic scale level, the surface tension modifications of nanofluids due to the nanoparticle dissipations were simulated by changing the fluid–fluid "particle" interaction strength G in Eq. (5.1). Two typical nanoparticles, hydrophobic and hydrophilic, were calculated with different G. The pure fluid was calculated as the baseline with $G = -130$, for which the surface tension is 15.8 μ ls^{-2}. For a 2D nanofluid drop with an initial radius of 50 lattices and 6 % nanoparticle volume fraction, the nanoparticles occupied 471 lattices (7854 lattices in total for the nanofluid drop with $R_0 = 50$ lu). By switching the particle–particle/particle–fluid interactions for these 471 lattices or their neighbor lattices to $G = -120$, the nanofluids with adding hydrophobic nanoparticles can be simulated, with a surface tension of 14.3 μ ls^{-2}. The nanofluid with hydrophilic nanoparticles, simulated with the particle–particle/particle–fluid interaction parameter of $G = -140$, has a surface tension of 17.6 μ ls^{-2}. The properties of the three types of fluids are listed in Table 5.1.

The adding of nanoparticles also modifies the rheological behavior of the base fluid, especially for the high nanoparticle loadings [1]. The rheology modification of nanofluids was simulated in the LBM by changing the relaxation time τ_f based on the local shear rates at every iterative step. The power-law rheological behavior was described by

$$\mu = \kappa \dot{\gamma}^{(n-1)}, \tag{5.4}$$

where κ is the viscosity coefficient, n is the rheological index, and $\dot{\gamma}$ is the local shear rate, which is calculated by the local shear rate tension $\mathbf{d}$,

$$\dot{\gamma}_{x,y} = \sqrt{2\mathbf{d}:\mathbf{d}}, \tag{5.5}$$

Table 5.1 Surface tension modification by nanoparticles with various wettabilities

Nanoparticle wettability	G	ρ_l	ρ_v	p_{sat}	σ
Hydrophobic	−120	524.37	85.7	25.56	14.3
Pure fluids	−130	611.27	76.16	23.57	15.8
Hydrophilic	−140	696.11	69.06	21.88	17.6

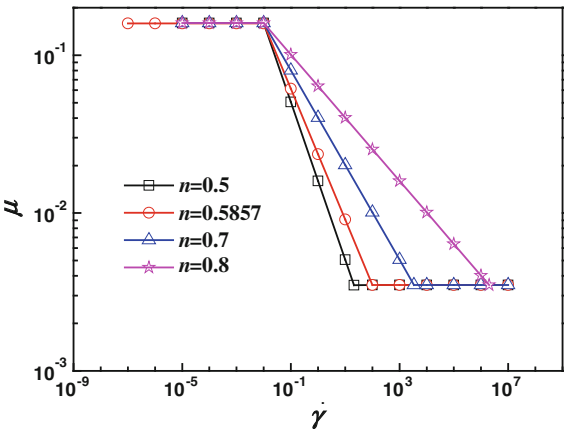

Fig. 5.3 Four shear-thinning nanofluids

Table 5.2 Four shear-thinning nanofluids ($\mu_0 = 0.16$, $\mu_\infty = 0.0035$)

n	Shear rate ranges	Parameters
$n = 0.5$	$10^{-2} < \dot{\gamma} < 21$	$k = 0.016$
$n = 0.5857$	$10^{-2} < \dot{\gamma} < 10^{2}$	$k = 0.0236$
$n = 0.7$	$10^{-2} < \dot{\gamma} < 3.4 \times 10^{3}$	$k = 0.04019$
$n = 0.8$	$10^{-2} < \dot{\gamma} < 2 \times 10^{6}$	$k = 0.06369$

where $\mathbf{d} = \frac{1}{2}(\nabla \mathbf{u} + \nabla \mathbf{u}')$.

The shear-thinning non-Newtonian behaviors were observed in most nanofluids [7]. The truncated power law (TPL) was used to describe the relationships of viscosities and shear rates. To examine the effects of rheology on the dynamic wetting, four shear-thinning nanofluids, with the equal viscosity boundaries ($\mu_0 = 0.16$, $\mu_\infty = 0.0035$) but different rheological indexes, are shown in Fig. 5.3. The TPL parameters of the four shear-thinning nanofluids are listed in Table 5.2.

It should be noted that the nanoparticle self-assembly is not considered when the bulk dissipations are discussed.

5.2.3.2 Structural Disjoining Pressure Due to Nanoparticle Self-assembly

Figure 5.4 shows two nanoparticle self-assembly modes for both the complete and the partial wetting. Nanoparticles likely deposit at the bottom (global deposition) or near the contact line (local deposition). The bottom and the contact line region depositions were regarded as two enhancement mechanisms of nanofluid dynamic wetting [7]. The structural disjoining pressure was used to explain the effects of nanoparticle deposition on the wetting kinetics [4]. A linear deposition rate with de = 0.007 lu^2/lt is given in Fig. 5.5, with which 141 fluid lattices transfer into solid

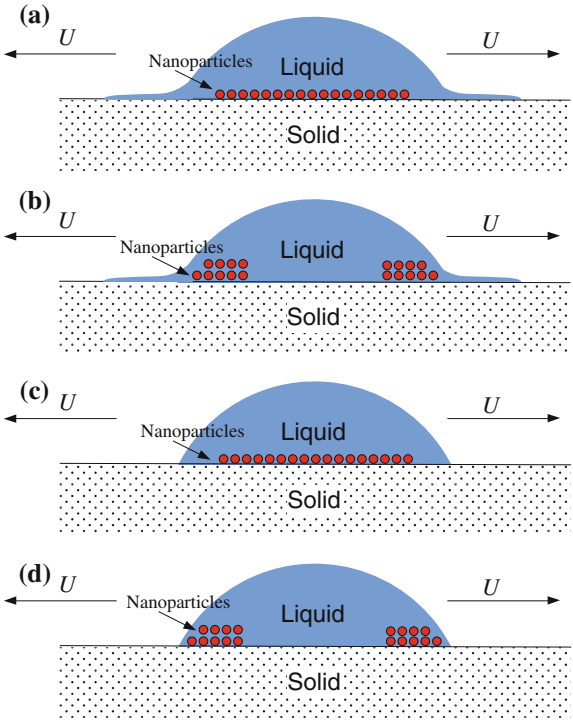

Fig. 5.4 Various nanoparticle self-assembly modes: **a** bottom deposition for the complete wetting; **b** contact line region deposition for the complete wetting; **c** bottom deposition for the partial wetting; **d** contact line region deposition for the partial wetting

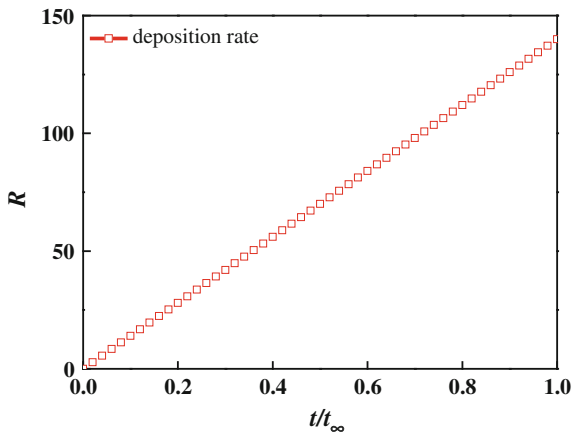

Fig. 5.5 Nanoparticle deposition rate

lattices on the lowest and the second lowest lattice layer, corresponding to 30 % nanoparticle deposit at t = 20,000 lt. As a nanoparticle lattice transfers into a solid lattice at the solid surface, a random particle lattice in the bulk liquid droplet changes into fluid lattice, correspondingly. For the bottom deposition cases, the nanoparticles are assumed to deposit from the center of drop bottom, and then

radiate outwards to the contact line region. If the lowest lattice layer was completely occupied by the deposited nanoparticles, the second lowest lattice layer transfers to the solid lattice from center to the droplet margin according to the given nanoparticle deposition rate. For the contact line deposition cases, the fluid lattices, with 1 lattice away from the contact line lattices, transfer to the solid lattices if they are occupied by the deposited nanoparticles. As the contact line move forwards, the second deposited nanoparticle appears at the location with 1 lattice away from the contact line. If more than two nanoparticles deposit at one time step, one nanoparticle deposits on the lowest layer, and the other deposits on the upper layer. It is noted that the bulk dissipation is neglected in the cases of nanoparticle sedimentation or self-assembly.

In nanoscale, the strong interactions between the substrate and the liquid molecule reduce the liquid pressure within the thin film and result in the disjoining pressure [38].

The disjoining pressure is defined as follows [39]:

$$\prod = -\frac{A_{\mathrm{SL}}}{6\pi\delta^3} \tag{5.6}$$

where A_{SL} is the Hamaker constant, and δ is the thickness of liquid film. The disjoining pressure decreases with increasing the liquid film thickness. As discussed in Chap. 3, nanoparticles self-assemble at the bottom or near the contact line region reducing the thickness of the thin film, leading to an additional disjoining pressure called structural disjoining pressure, which facilitates the motion of the contact line. The disjoining pressure can also be calculated using the pressure equilibrium on the liquid–vapor interface [40],

$$\prod = \rho k_{\mathrm{B}} T \ln\left(\frac{p_{\mathrm{v}}}{p_{\mathrm{sat}}}\right) \tag{5.7}$$

where p_{v} is the vapor pressure, p_{sat} is the saturated pressure, k_{B} is the Boltzmann constant, T is the temperature, and ρ is the vapor density.

Figure 5.6 shows the condensation of vapor with different saturabilities within the capillary tube. The thickness of condensed liquid film increases with increasing vapor saturability. Figure 5.7 shows the comparison of the disjoining pressures calculated from Eq. (5.6) using the LBM-simulated film thickness with the results from Eq. (5.7) using the vapor saturability. The good agreement indicates that the LBM can predict the disjoining pressure which occurs in nanoscale. Figure 5.7 also indicates that the disjoining pressure only exists in the thin film with less than 2 lattices in thickness. The deposited nanoparticles reduce the thin film thickness and result in the structural disjoining pressure.

The individual effect of the surface tension, rheology, and the structural disjoining pressure was studied to examine the bulk and local dissipation effects due to nanoparticle motion on the nanofluid dynamic wetting.

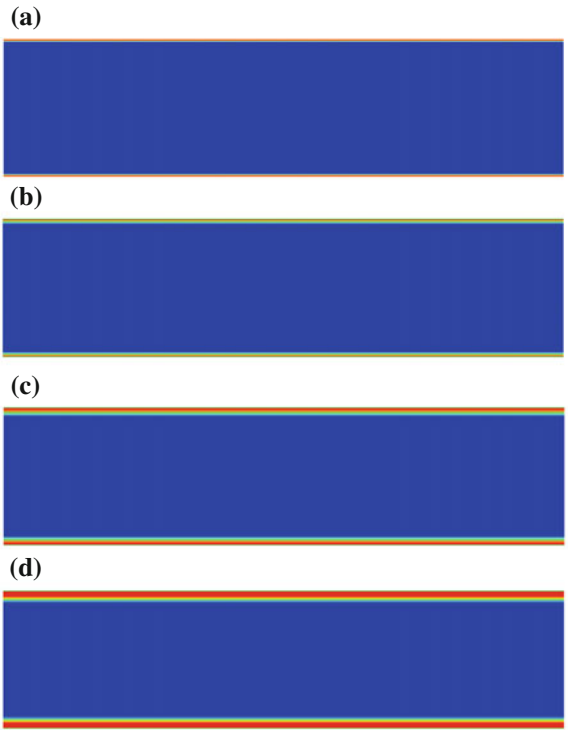

Fig. 5.6 Condensation of vapor within capillary tube: **a** vapor saturability φ = 5 %; **b** φ = 10 %; **c** φ = 15 %; **d** φ = 20 %

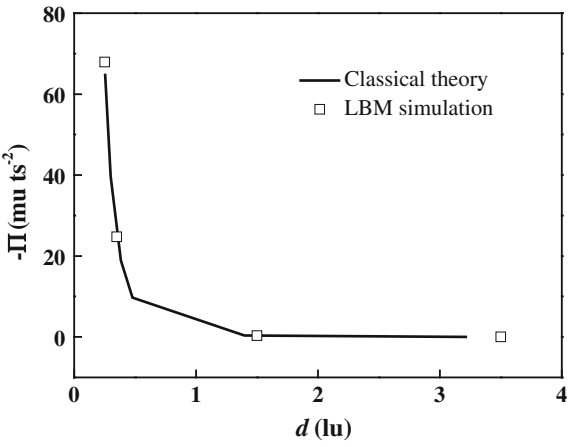

Fig. 5.7 Comparison of disjoining pressure calculated with simulated film thickness (LBM simulation) and the calculation with the given vapor saturation

5.3 Results and Discussions

5.3.1 *Bulk Dissipation Due to the Surface Tension Modification*

Figure 5.8 shows the pure fluid and nanofluid dynamic wetting at t = 18,000 lt (lattice time). The nanofluids with hydrophobic nanoparticle, as shown in Fig. 5.8a, prefer to spread completely, while the pure fluids (Fig. 5.8b) and the nanofluids with hydrophilic nanoparticles (Fig. 5.8c) show the partial wetting behavior. The equilibrium contact angle of the nanofluids with hydrophilic nanoparticles is larger than that of pure fluids. The precursor layer was only observed in the nanofluids with hydrophobic nanoparticles. The nanoparticle wettability is responsible for the nanofluid surface tension. The surface tension of base fluids decreases with adding hydrophobic nanoparticles, but increases with adding hydrophilic nanoparticles [38]. According to the contact line motion driven force, $F = \sigma_{SL} - \sigma_{SV} - \sigma_{LV}\cos\theta$, the spreading increases with decreasing the liquid–vapor surface tension.

Figure 5.9a shows the non-dimensional spreading radius variation with spreading time, in which R_0 = 50 lu and t_∞ = 20,000 lt. Both the pure fluid and the nanofluid with hydrophilic nanoparticles have reached the equilibrium stages. The equilibrium non-dimensional radius of the pure fluid droplet was R/R_0 = 1.653 after t/t_∞ = 0.530, while R/R_0 = 1.384 for the nanofluid drop with hydrophilic nanoparticles after t/t_∞ = 0.445. The nanofluid drop with hydrophobic nanoparticles has a spreading radius of 2.529 and keep spreading after t_∞ = 20,000 lt. The logarithmic results in Fig. 5.9b indicate the two stages of the droplet spreading, the initial fast spreading stage and the slow spreading stage. The two stage partial wetting was also reported in the Ref. [41]. The slow spreading stages occupy most of the spreading time, for insistence, 92 % for the hydrophobic nanoparticle fluids,

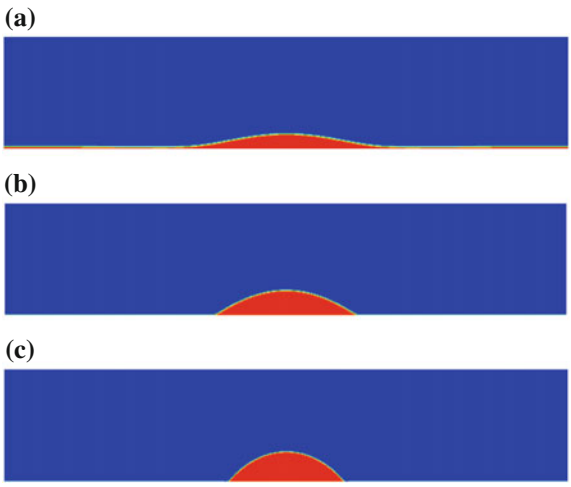

Fig. 5.8 Effects of nanoparticle wettability on the dynamic wetting of nanofluids (t = 18,000 lt): **a** hydrophobic nanoparticles; **b** pure fluids; **c** hydrophilic nanoparticles

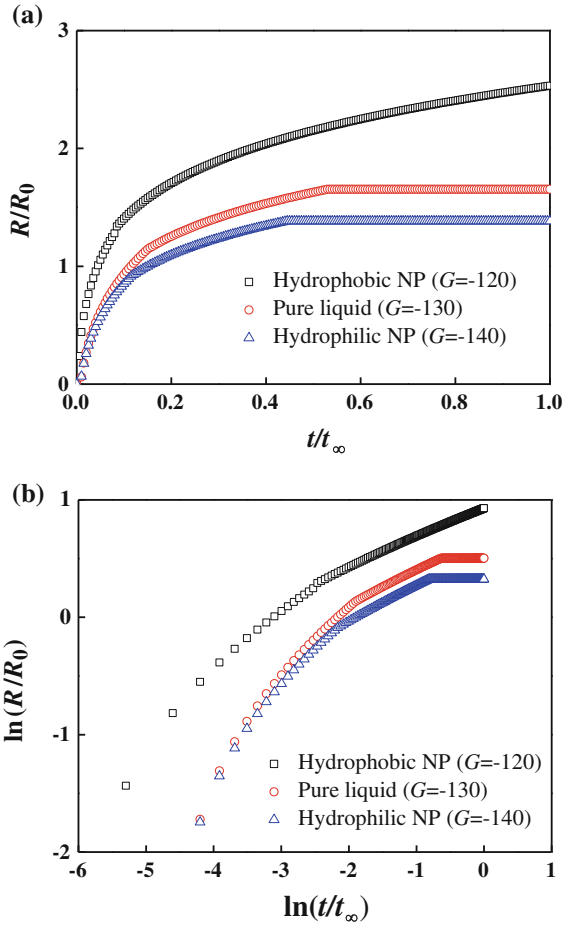

Fig. 5.9 Non-dimensional spreading radii versus spreading time for the three fluid droplets

85 % for pure fluids, and 89 % for hydrophilic nanoparticle fluids. The spreading laws of the three fluid droplets are fitted as shown below:

$$\begin{cases} R' - t'^{0.145} & (G = -120) \\ \begin{cases} R' - t'^{0.261} & (t' < 0.145) \\ R' - t'^{0.142} & (t' > 0.145) \end{cases} & (G = -130) \\ \begin{cases} R' - t'^{0.241} & (t' < 0.115) \\ R' - t'^{0.140} & (t' < 0.115) \end{cases} & (G = -140) \end{cases} \tag{5.8}$$

where the spreading exponent of the complete wetting (CW) ($G = -120$), $\alpha = 0.145$, is larger than 1/7, and the spreading exponent of 2D Newtonian fluid droplets is predicted by the hydrodynamic model. The results indicate that the additional hydrophobic nanoparticles, which acting like surfactants, greatly facilitate the dynamic wetting, while hydrophilic nanoparticles inhibit the droplet spreading. The

results also indicate that the dynamic wetting by nanofluids with hydrophobic nanoparticles deviate from Newtonian spreading behaviors. The effects of rheology on the dynamic wetting should be examined.

5.3.2 Bulk Dissipation Due to the Rheology Modification

To examine the effects of rheology on the nanofluid dynamic wetting, two additional types of fluids were simulated. One fluid is created with $G = -130$ for all particle–particle/particle–fluid/fluid–fluid interactions and the rheological exponent of $n = 0.8$, corresponding to a shear-thinning non-Newtonian fluid without nanoparticles. The other fluid is simulated with $G = -120$ and $n = 0.8$, corresponding to a shear-thinning non-Newtonian fluid with hydrophobic nanoparticles. Figure 5.10 shows the effects of surface tension and rheology modification on the dynamic wetting of nanofluids. The results indicate that the dynamic wetting by nanofluids is dominated by both the surface tension and the rheological properties. The dynamic wetting capacity is underestimated if the rheology modification is neglected, as compared $G = -120$, $n = 0.8$ with $G = -120$, $n = 1$. However, if the surface tension modification is neglected, the nanofluids exhibit the partial wetting behavior, as shown in the comparison between $G = -120$, $n = 0.8$ and $G = -130$, $n = 0.8$. The modification of surface tension is more related to the wettability capacity which can be characterized by the spreading coefficient, $S = \sigma_{SL} - \sigma_{SV} - \sigma_{LV}$. The fluids exhibit CW behaviors if $S > 0$ while partial wetting for $S < 0$. Although the rheology is modified for the fluids with $G = -130$ and $n = 0.8$, the fluids still exhibit partial wetting behaviors. Therefore, both the modifications of surface tension and rheology contribute to the dynamic wetting by nanofluids.

The effects of rheology on the dynamic wetting are further examined by changing the rheological index. The adding nanoparticles are hydrophobic

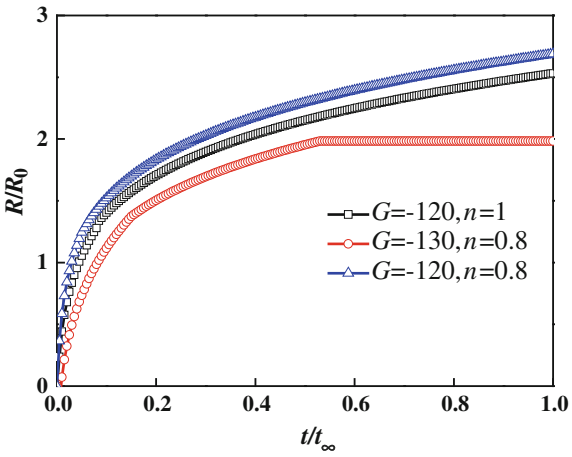

Fig. 5.10 Effects of surface tension and rheology on the dynamic wetting of nanofluids

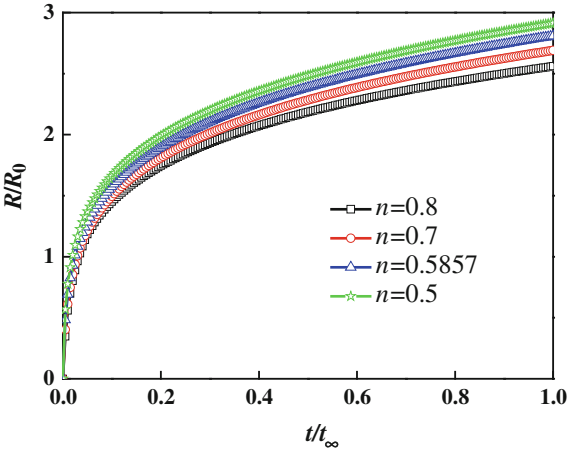

Fig. 5.11 Effects of rheological indexes on the dynamic wetting of nanofluids ($G = -120$)

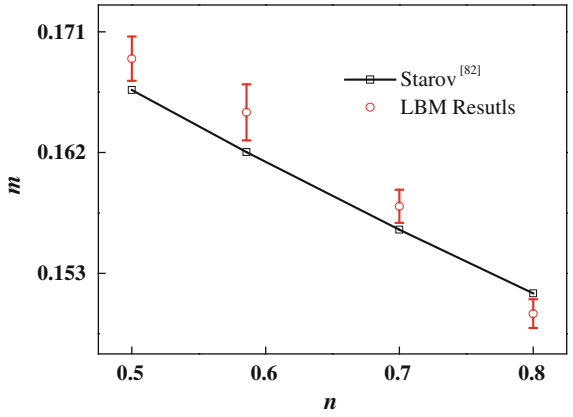

Fig. 5.12 Comparison of LBM results and Starov's model for the spreading exponents versus rheological index

($G = -120$). As shown in Fig. 5.11, the dynamic wetting capability increases with decreasing the rheological indexes. The dynamic wetting is enhanced due to the weaker viscous dissipation. Figure 5.12 shows the relation of the spreading exponents and the rheological indexes. The LBM results agree with the Starov's non-Newtonian dynamic wetting model [42], in which $m = n/(5 + 2n)$ for a 2D droplet spreading.

5.3.3 *Local Dissipation Due to Structural Disjoining Pressure*

Figure 5.13 shows the effects of nanoparticle self-assembly on the dynamic wetting of nanofluids at $t = 20{,}000$ lt, in which CW is the CW (by adding hydrophobic

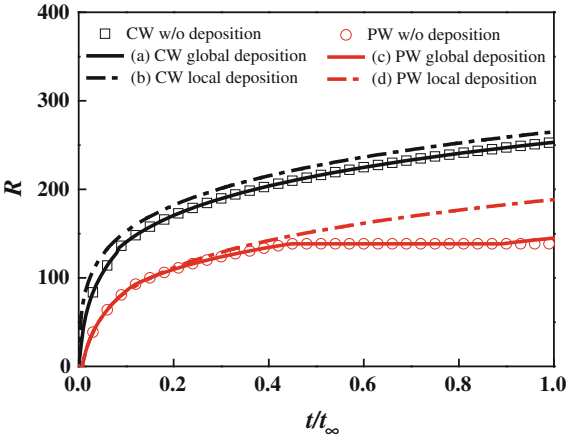

Fig. 5.13 Effects of nanoparticle self-assembly on the dynamic wetting process

nanoparticles), PW is the partial wetting (by adding hydrophilic nanoparticles), and w/o presents without deposition. It should be noted that the rheology modification is not considered here because the rheology does not change the wetting behaviors qualitatively as discussed in Sect. 5.3.2. For the CW drop, the globally deposited nanoparticles do not affect the thin film thickness in the vicinity of the contact line region during the nanofluid droplet spreading, even for the 30 % deposition. Therefore, the deposition has few effects on the dynamic wetting process. However, the local deposition in the vicinity of the contact line region reduces the thin film thickness, leading to an additional disjoining pressure. Therefore, the local deposition enhances the dynamic wetting process from the beginning of wetting process. For the partial wetting droplet, the globally deposited nanoparticles do not affect the wetting kinetics at the beginning. At the last stage ($t/t_\infty > 0.9$), when the deposited nanoparticles change the thin film thickness, the spreading is enhanced due to the nanoparticle deposition. For the local deposition, since the dynamic contact angle is large, the nanoparticle deposition has few effects on the dynamic wetting at the beginning stage. However, the deposition strongly affects the dynamic wetting at the last stage, since the deposition of nanoparticles reduces the thin film thickness for the small contact angle cases, leading to an additional structural disjoining pressure near the contact line region. Figure 5.14 shows the disjoining pressure in the vicinity of the contact line region for the four nanoparticle deposition modes. The disjoining pressure difference between the contact line and the bulk liquid region is responsible for the motion of contact line. For the CW, the nanoparticle depositions have few effects on the disjoining pressure. However, for the partial wetting, the depositions strongly affect the disjoining pressure in the vicinity of the contact line region. Therefore, the effects of nanoparticle deposition for the partial wetting are more significant than that of CW. For the CW, the disjoining pressure in the precursor layer balances the structural disjoining pressure due to the self-assembly of nanoparticles, hence the nanoparticle self-assembly has few effects on the dynamic wetting.

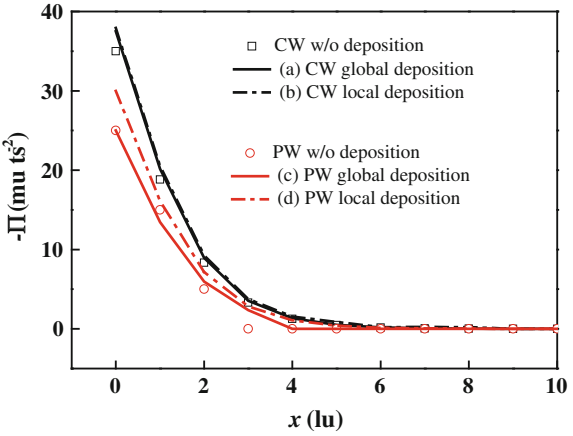

Fig. 5.14 Disjoining pressure in the vicinity of contact line region for the four nanoparticle deposition modes (t = 20,000 lt)

5.4 Conclusions

The multiphase LBM was used to study the nano-scale dissipation effects on the macroscale dynamic wetting process. The microscopic dissipation effects include the surface tension and the rheology modifications due to the nanoparticle motion in the bulk liquid, as well as the structural disjoining pressure due to the nanoparticle deposition near the contact line region.

1. The adding of hydrophobic nanoparticle facilitates the dynamic wetting while the hydrophilic nanoparticles deteriorate the dynamic wetting. The partial wetting process was divided into two stages. The spreading exponent of the slow stage consists with the hydrodynamic model prediction;
2. The shear-thinning non-Newtonian behavior due to the adding of nanoparticle enhances the dynamic wetting of nanofluids. The wetting capability increases with the decreasing rheological indexes. The relation of the spreading exponent and the rheological index agree with the Starov's model.
3. The nanoparticle global deposition has few effects on the dynamic wetting, while the local deposition strongly affects the dynamic wetting process. For the partial wetting drop, the structural disjoining pressure due to the self-assembly of nanoparticle in the vicinity of the contact angle region greatly facilitates the contact line motion.

References

1. Chen HS, DingYL TanCQ (2007) Rheological behaviour of nanofluids. New J Phys 9:367
2. Tanvir S, Li Q (2012) Surface tension of nanofluid-type fuels containing suspended nanomaterials. Nanoscale Res Lett 7:226–236
3. Wasan DT, Nikolov AD (2003) Spreading of nanofluids on solids. Nature 423:156–159

4. Kondiparty K, Nikolov AD, Wu S et al (2011) Wetting and spreading of nanofluids on solid surfaces driven by the structural disjoining pressure: statics analysis and experiments. Langmuir 27:3324–3335
5. Kondiparty K, Nikolov AD, Wasan DT et al (2012) Dynamic spreading of nanofluids on solids part I: Experimental. Langmuir 28:14618–14623
6. Liu KL, Kondiparty K, Nikolov AD et al (2012) Dynamic spreading of nanofluids on solids part II: modeling. Langmuir 28:16274–16284
7. Sefiane K, Bennacer R (2009) Nanofluids droplets evaporation kinetics and wetting dynamics on rough heated substrates. Adv Colloid Interface Sci 147–148:263–271
8. Moffat JR, Sefiane K, Shanahan MER (2009) Effect of TiO_2 nanoparticles on contact line stick-slip behavior of volatile drops. J Phys Chem B 113:8860–8866
9. Murshed SMS, Nieto de Castro CA, Lourenco MJV et al (2007) A review of boiling and convective heat transfer with nanofluids. Renew Sust Energy Rev 15:2342–2354
10. Wen DS (2008) Mechanisms of thermal nanofluids on enhanced critical heat flux (CHF). Int J Heat Mass Transf 51:4958–4965
11. Sefiane K (2006) On the role of structural disjoining pressure and contact line pinning in critical heat flux enhancement during boiling of nanofluids. Appl Phys Lett 89:044106
12. Fattahi E, Farhadi M, Sedighi K (2011) Lattice Boltzmann simulation of natural convection heat transfer in nanofluids. Int J Therm Sci 50:137–144
13. Lai FH, Yang YT (2011) Lattice Boltzmann simulation of natural convection heat transfer of Al_2O_3/water nanofluids in a square enclosure. Int J Therm Sci 50:1930–1941
14. Yang YT, Lai FH (2011) Numerical study of flow and heat transfer characteristics of alumina-water nanofluids in a microchannel using the Lattice Boltzmann method. Int Commun Heat Mass Transf 38:607–614
15. Nabavitabatabayi M, Shirani E, Rahimian MH (2011) Investigation of heat transfer enhancement in an enclosure filled with nanofluids using multiple relaxation time Lattice Boltzmann modeling. Int Commun Heat Mass Transf 38:128–138
16. Bararnia H, Hooman K, Ganji DD (2011) Natural convection in nanofluids-filled portioned cavity: the Lattice-Boltzmann method. Numer Heat Transf A 59:487–502
17. Kefayati GR, Hosseinizadeh SF, Gorji M (2012) Lattice Boltzmann simulation of natural convection in an open enclosure subjugated to water/copper nanofluid. Int J Therm Sci 52:91–101
18. Kefayati GR, Hosseinizadeh SF, Gorji M (2011) Lattice Boltzmann simulation of natural convection in tall enclosures using water/SiO_2 nanofluid. Int Commun Heat Mass Transf 38:798–805
19. He YR, Qi C, Hu YW (2011) Lattice Boltzmann simulation of alumina-water nanofluid in a square cavity. Nanoscale Res Lett 6:184
20. Nemati H, Farhadi M, Sedighi K (2010) Lattice Boltzmann simulation of nanofluid in lid-driven cavity. Int Commun Heat Mass Transf 37:1528–1534
21. Xuan YM, Yu K, Li Q (2005) Investigation on flow and heat transfer of nanofluids by the thermal Lattice Boltzmann model. Prog Comput Fluid Dyn 5:13–19
22. Xuan YM, Li Q, Yao ZP (2004) Application of Lattice Boltzmann scheme to nanofluids. Sci China Ser E 47:129–140
23. Xuan YM, Yao ZP (2005) Lattice Boltzmann model for nanofluids. Heat Mass Transf 3:199–205
24. Zhou LJ, Xuan YM, Li Q (2010) Multiscale simulation of flow and heat transfer of nanofluid with Lattice Boltzmann method. Int J Multiph Flow 36:364–374
25. Shih CH, Wu CL, Chang LC et al (2011) Lattice Boltzmann simulations of incompressible liquid-gas systems on partial wetting surfaces. Philos Trans R Soc Lond Series A 369:2510–2518
26. Joshi AS, Sun Y (2010) Wetting dynamics and particle deposition for an evaporating colloidal drop: a Lattice Boltzmann study. Phys Rev E 82:041401
27. Yu Y, Liu YL (2008) Lattice-Boltzmann models simulation of wetting modes on the surface with nanostructures. J Comput Theor Nanosci 5:1377–1380

28. Yan YY, Zu YQ (2007) A Lattice Boltzmann method for incompressible two-phase flows on partial wetting surface with large density ratio. J Comput Phys 227:763–775
29. Davies AR, Summers JL, Wilson MCT (2006) On a dynamic wetting model for the finite-density multiphase Lattice Boltzmann method. Int J Comput Fluid Dyn 20:415–425
30. Zou Q, Hou S, Chen S (1995) An improved incompressible Lattice Boltzmann model for time-independent flows. J Stat Phys 81:35–48
31. Shan XW, Chen HD (1993) Lattice Boltzmann model for simulating flows with multiple phases and components. Phys Rev E 47:1815–1819
32. Shan XW, Chen HD (1994) Simulation of nonideal gases and liquid-gas phase-transitions by the Lattice Boltzmann-equation. Phys Rev E 49:2941–2948
33. Shan XW, Doolen GD (1995) Multicomponent Lattice-Boltzmann model with interparticle interaction. J Stat Phys 81:379–393
34. He XY, Doolen GA (2002) Thermodynamic foundations of kinetic theory and Lattice Boltzmann models for multiphase flows. J Stat Phys 107:309–328
35. Sukop MC, Thorne DT Jr (2007) Lattice Boltzmann modeling. Springer, New York
36. Martys NS, Chen HD (1996) Simulation of multicomponent fluids in complex three-dimensional geometries by the Lattice Boltzmann method. Phys Rev E 53:743–750
37. Lu G, Hu H, Duan YY et al (2013) Wetting kinetics of water nano-droplet containing non-surfactant nanoparticles: a molecular dynamics study. Appl Phys Lett 103:253104
38. Lu G, Duan YY, Wang XD (2014) Surface tension, viscosity, and rheology of water-based nanofluids: a microscopic interpretation on the molecular level. J Nanopart Res 16:2564
39. Israelachviliv JN (2011) Intermolecular and surface forces, 3rd edn. Academic Press, Burlington
40. Carry VP, Wemhoff AP (2006) Disjoining pressure effects in ultra-thin liquid films in micropassages—comparison of thermodynamic theory with predictions of molecular dynamics simulations. ASME J Heat Transf 128:1276–1284
41. de Ruijter MJ, de Coninck J, Oshanin G (1999) Droplet spreading: partial wetting regime revisited. Langmuir 15:2209–2216
42. Starov VM, Tyatyushkin AN, Velarde MG et al (2003) Spreading of non-Newtonian liquids over solid substrates. J Colloid Interface Sci 257:284–290